Journal of Applied Research and Technology

www.jart.icat.unam.mx

Journal of Applied Research and Technology 22 (2024) 806-815

Original

Obstacle arrangements effect on the mixed convection in an enclosure with movable top surface

A. M. Shaker[a] • N. J. Yasin[a] • H. A. Ameen[a] • A. S. Abedalh[b]*

[a]*Technical University, Baghdad, Iraq*
[b]*Northern Technical University, Mosul, Iraq*

Received 05 22 2024; accepted 08 01 2024
Available 12 31 2024

Abstract: The flow finds extensive application in coating, drying, and mixing processes. The temperature and velocity distribution inside a rectangular enclosure that is driven by a lid were examined using a finite volume numerical method. Five adiabatic cylindrical obstacles were mounted within the cage measures 25 cm in width and 30 cm in length. The right and left walls enclosure is each fully insulated, the top wall was cooled isothermally at Tc and moved at variable speed of U, and the bottom wall was kept at Th using water as a working fluid. Three types of an obstacle with equal area were utilized in this study they were, circle triangle and square. The results showed that the average Nusselt number increases by 10.4%,12%, 16%, and 19% compared with that of without the obstacle for radius values (r=0.5,1,1.5 and 2 cm) respectively. The results indicate that obstacles can be very useful in achieving a higher rate of heat transfer compared to the enclosure without obstacles. Also, as opposed to a situation without barriers, the results demonstrate that the existence of obstructions causes an increase in the average Nusselt number. When compared to triangular and square shapes, the obstacle with a circular shape has a larger average Nusselt number. Furthermore, the enhancement percentage of Nusselt number was calculated to be 16, 13, 11 % for obstacle models of circle have a radius of 1 cm, triangle and square of 1 cm (major dimension) respectively comparing with that of no obstacles.

Keywords: Enclosure, obstacles, movable wall, square lid-driven, mixed convection

*Corresponding author.
E-mail address: ayad.selman@ntu.edu.iq (A. S. Abedalh).
Peer Review under the responsibility of Universidad Nacional Autónoma de México.

1. Introduction

The enclosure with lid-driven flow is widely used in mixing, coating, and drying applications and constitutes a significant factor in the study of heat transfer rates and fluid fields. A significant phenomenon in science and engineering systems, mixed convection is used in a wide range of applications, including heat exchangers high-thermal performance building, insulation, home ventilation, and solar energy applications. Mamun et al. (2010) investigated the properties of mixed convection heat transfer in a vented square cavity with a heated hollow cylinder. The heated hollow cylinder was positioned in the cavity's center. It was assumed that the cavity wall was adiabatic and the flow entered the cavity at the bottom of the left wall through the inlet and left at the top of the right wall. The current investigation focused on the effects of the cylinder's thermal conductivity and diameter in the cavity. Kahveci and Öğüt (2011) studied numerically the mixed convection of water-based nanofluids in a square enclosure powered by a lid and equipped with a heater that provides a constant heat flux. For the heater lengths of 0.25, 0.50, and 0.75, the computational results were obtained. The Reynolds number was changed to ensure that the Richardson number has values between 0.1 and 10, but the Grashof number was maintained at a constant 104. The findings demonstrate that when the heater's length and Richardson number are reduced, the rate of heat transmission will rise significantly. Islam et al. (2012) examined the laminar mixed flow by numerical characteristics in a square cavity with a square obstruction that was heated isothermally. The cavity's four surfaces, including the lid, are maintained at a cold temperature Tc, while the blockage is maintained at a hot temperature Th, under all circumstances. The geometrical of the problem and flow characteristics include the blockage ratio (B), blockage placement eccentricities, Reynolds number (Re), Grashof number (Gr), and Richardson number (Ri). Khanafer and Aithal (2013) conducted a numerical analysis for the mixed convection flow and heat transmission properties in a circular hollow driven by a lid. The study attempts to demonstrate how the non-dimensional radius of the cylinder, its position, and the Richardson number affect the transport phenomena inside the cavity. The results indicated that when compared to a case without a cylinder, the average Nusselt number increases when the cylinder was included. Experimental study of mixed convection in an enclosure with a cold movable top wall and hot bottom wall investigation by Yasin et al. (2014). The differential temperature of the bottom and top walls changed several times in order to accurately characterize the temperature distribution over a considerable range of Richardson number. Adjustable aspect ratio box was built as a test rig to determine the effects of Richardson number and aspect ratio on the flow behavior of the air inside the enclosure. The flow fields and the average Nusselt number profiles were presented in this work. The results show that, at a constant value of the Richardson number, average Nusselt number (Nuav.) increases with aspect ratio. Furthermore, as Richardson number decreases, the time period decreases with constant values of aspect ratio. Moumni et al. (2015) investigated the flow and heat transmission of mixed convection-based water-containing (Cu, Ag, Al2O3, and TiO2) nanoparticles quantitatively. Two independent heat sources were located on the bottom wall of the enclosure, while the vertical moving walls and ceiling were maintained at a constant temperature. The remaining border parts of the bottom wall remain insulated. The flow was driven by the buoyancy force and the two opposing vertical walls flowing in the same direction. The study centers on the impacts of the monitoring parameters within designated ranges, such as the materials of the nanoparticles, the locations of the two heat sources, the solid volume percentage ($0 \le \varphi \le 0.2$), Reynolds ($1 \le Re \le 100$) and Richardson numbers ($1 \le Ri \le 20$). Morshed et al. (2015) studied two isothermally heated square internal obstructions in a lid-driven square cavity using numerical laminar mixed convection. The cavity's upper lid was traveling steadily to the right. The temperature of the cavity's walls was kept fixed, but the two obstructions were kept at a steady degree of heat. It was shown that when blockages were positioned diagonally, they had superior heat transmission characteristics, and that the average Nusselt number on the blockage surfaces varied considerably as a result of the placement adjustments. When the Reynolds number is low, forced convection predominates in the flow and has minimal effect on the efficiency of heat transmission. Boidin et al. (2016) conducted the mixed convection of the nanofluid in a two-sided lid-driven square cavity with two triangular heat sources was the subject of a numerical research. A constant temperature is maintained by cooling the left and right walls, and thermal insulation is provided for the upper and bottom moving walls. The rate of heat transmission rises with increasing Richardson number (Ri) and volume percentage of nanoparticles ($\boldsymbol{\varphi}$). The heat transfer rate rises as the diameter of the nanoparticle decreases, reaching its maximum values at a diameter of 25 nm. When several types of nanofluids are utilized, nonsignificant variations in the heat transfer rate are seen in all Richardson values. Messaoud et al. (2017) curried out a numerical analysis to investigate the combined impacts of lid movement and buoyancy on the parameters of heat transfer and flow for mixed convective flow inside an arc-shaped cavity controlled by the lid. The numerical conclusions are illustrated with streamlines, isotherms, velocity profiles, and average Nusselt number along the bottom wall. The comparisons showed that increasing the Reynolds and Grashof numbers improves heat transmission for all types of alveoli. Ouahouah et al. (2019) examined numerically the

TiO2-water nanofluid laminar mixed convection around a heated obstruction in a square cavity with moving vertical walls. The following parameters on the hydrodynamic and thermal properties around a heated obstacle in the enclosure were employed, the Reynolds number (50 ≼ Re ≼ 500), the Richardson number (0 ≼Ri≼ 10), and the volume fraction of nanoparticles (0% ≼ ϕ≼ 5%). Gangawane et al. (2019) explored the heat transfer and two-dimensional, steady and laminar mixed convective fluid circulation in a square lid-driven cavity affected by the shift in the triangle block's thermal condition with constant heat flux (CHF). The results showed that the centered block position (Ly = 0.5) had higher heat transfer rates than the other two (Ly = 0.25, 0.75). Yousefzadeh et al. (2020) examined the laminar mixed convection heat transfer inside an open square cavity with various heat transfer areas by using numerical modeling. The cavity is filled with cold fluid in the suggested geometry. A hot, round isothermal heat source is located in the center of the hollow. Solid silver nanoparticles with volume fractions (ϕ) of 0, 2, and 4% are added to water to increase heat transfer rate. Backflows can alter the heat transfer mechanism but do not enhance heat transfer by increasing fluid velocity. The effects of velocity gradients and the extension of the velocity boundary layer intensify as the fluid velocity decreases, and the friction coefficient reaches its maximum value. Shirani et al. (2021) examined the heat transfer numerically in a lid-driven square cavity with four revolving cylinders moving harmonically for a range of parameters that including the Reynolds number (86.2≤Re≤862), the volume percent of the nanoparticles (0≤ φ ≤ 0.03), and the Richardson number (0.1 ≤ Ri ≤ 10). The container was full of water-Cu nanofluids. The effect of introducing nanoparticles to pure water is another finding from. The thermos-physical characteristics of pure water were generally enhanced by increasing the concentration of nanoparticles in the solution. According to the overview above, numerical techniques for solving the governing equations of the lid driven cavity of without obstacle are used in most investigations about mixed convection in enclosures. The prior review of the literatures demonstrates that there is no focused on the type and formations of the obstacle inside the cavity how rarely is used in these investigations. The present work was used five adiabatic cylindrical obstacles within the cage measure 25 cm in width and 30 cm in length. The right and left walls enclosure is each fully insulated, the top wall is cooled isothermally at Tc and moves at variable speed of U, and the bottom wall was kept at Th and the water was used as a working fluid. Three types of an obstacle of [circle (r=0.5,1,1.5 and 2 cm), triangle and square] was utilized in this study.

2. Numerical Analysis and simulation

A numerical analysis was conducted to examine the numerical results to confirm the effectiveness and heat recovery results that were acquired. CFD is a computer-based method utilized to solve and investigate complex difficult, costly, and time-consuming problems and used mainly for modeling the behavior of systems including fluid flow, heat transfer, and other physical processes (Moukalled et al. 2016; Abedalh &. Mohammed, 2023). In this section, the numerical model of stable turbulent mixed convection in a two-dimensional enclosure partitioned by conducting obstacles was examined using ANSYS- FLUENT V. 20.0. Numerical solutions were obtained for various Reynolds numbers, Grashof numbers, and the forms of the obstacles inside the enclosure. The physical model represents an enclosure containing water inside. The enclosure is heated from below and insulated from its two side walls. The enclosure with oscillating motion by horizontal movement of the top cold wall. The assumptions used to solve the flow and heat transfer equations (mass, momentum, and energy equations) and the development of the model are a Two-dimensional turbulent steady-state flow field (Yasin et al., 2019). The water is incompressible, the side walls are adiabatic, the density of the momentum equation is varied vertically using the Boussinesq approximation, the effect of gravity is minimal, and there is no heat loss. The continuity (mass conservation) governing equation Navier-Stokes equations for the flow field has been solved (Shaalan et al., 2021; Abedalh et al., 2021):

The continuity equation is given by:

$$\frac{\partial u}{\partial x} + \frac{\partial v}{\partial y} = 0 \tag{1}$$

The momentum equation in the x-direction is given by:

$$\mathrm{u}\frac{\partial \mathrm{u}}{\partial \mathrm{x}} + \mathrm{v}\frac{\partial \mathrm{u}}{\partial \mathrm{y}} = -\frac{1}{\rho eff}\frac{\partial \mathrm{p}}{\partial \mathrm{x}} + \frac{\mu_{eff}}{\rho_{eff}}\left(\frac{\partial^2 \mathrm{u}}{\partial \mathrm{x}^2} + \frac{\partial^2 \mathrm{u}}{\partial \mathrm{y}^2}\right) \tag{2}$$

The momentum equation in the y-direction is given by Abedalh et al. (2023), Hussein et al. (2023) and Abdallah et al., 2022):

$$\mathrm{u}\frac{\partial \mathrm{v}}{\partial \mathrm{x}} + \mathrm{v}\frac{\partial \mathrm{v}}{\partial \mathrm{y}} = -\frac{1}{\rho_{\mathrm{eff}}}\frac{\partial \mathrm{p}}{\partial \mathrm{y}} + \frac{\mu_{\mathrm{eff}}}{\rho_{\mathrm{eff}}}\left(\frac{\partial^2 \mathrm{v}}{\partial \mathrm{x}^2} + \frac{\partial^2 \mathrm{v}}{\partial \mathrm{y}^2}\right) + \frac{\mathrm{g}(\rho_{\mathrm{eff}} - \rho)}{\rho_{\mathrm{eff}}} \tag{3}$$

Using the Boussinesq approximation equation is formed by:

$$\rho = \rho_{eff}\left(1 - \beta(T - T_c)\right) \tag{4}$$

where the buoyancy force term, or body force per unit volume in the y-direction, is denoted by the symbol $\beta g(T-T_c)$. The macroscopic energy equation is provided by: Considering the prior section's assumptions on radiative effects, viscous dissipation, and the insignificant work caused by pressure change (Yunus, 2003) :

$$\rho c_p \left(u \frac{\partial T}{\partial x} + v \frac{\partial T}{\partial y} \right) = k \left(\frac{\partial^2 T}{\partial x^2} + \frac{\partial^2 T}{\partial y^2} \right) \quad (5)$$

The geometry considered in this study is a two-dimensional enclosure outline. The enclosure with a length of 30 cm and a width of 25 cm was built and has five interior cylinders with diameters of 1, 1.5, and 2 cm. It is assumed that the fluid flow is laminar, incompressible, and has very little viscous dissipation. The top wall of the enclosure moves at a constant speed of U and is isothermally cooled at Tc. Additionally, the enclosure's bottom wall is kept at a hot temperature of T_h such that T_h is higher than T_c. The walls of the enclosure are perfectly insulated and the obstacles are adiabatically insulated as schematically shown in Fig. 1. Apart from the fluctuation in density with temperature (Boussinesq approximation), which gives rise to the buoyant forces, all the thermos-physical parameters of the fluid are presumed constant. The thermos-physical properties of the fluid are assessed at the ambient temperature, (Ti), which is always equal to 300 K.

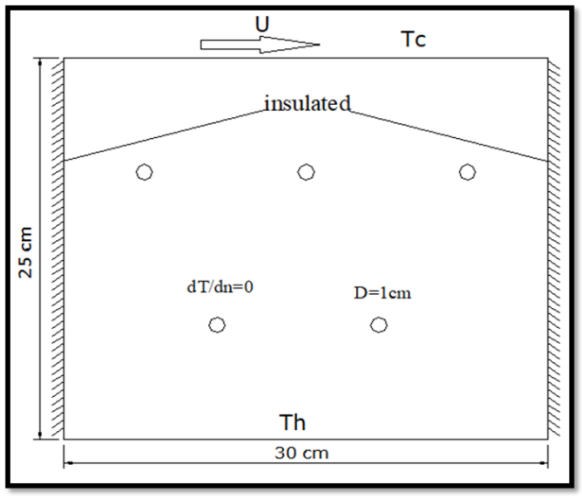

Figure 1. Geometric dimensions of the enclosure employed in the numerical simulation.

The mesh generation process began after the geometry was completed. After sketching all the geometrical elements of the enclosure in the Auto-CAD program, the ANSYS CFD meshing software begins with advanced CAD/geometry reading and builds the mesh. The most important of which are the mesh type (unstructured or structured) and the relative size of each computational cell. The most frequent cell shape for two-dimensional unstructured grids is a triangle, whereas cells for structured grids are quadrilaterals (2D). Unstructured grids are employed in the current investigation since they typically work well for complex geometries. Due to the high number of operations performed per node, there is also a significant computational overhead.

Increasing the resolution and running the simulation again is the standard procedure for testing for grid independence. The original grid is probably fine if the findings do not drastically alter. If, however, there are significant differences between the two responses, the first grid was probably not resolved enough. Computations have been carried out for four selected grid sizes (i.e., 23186, 703974, 116790,183934, and 215239), the summary of the grid independence test findings is presented in Table (1). It was observed that the 183934 and 215239 nodes produced almost identical results with a percentage error of 0.08%. From the results in Fig. 2, it can be explained that there is a significant disparity in the results and that as the number of elements increases, the results begin to converge. After meshing (d) and (e) the difference in the result value is very small, the (e) mesh has been chosen. Fig. 3 explains mesh dependency for an arbitrary case.

Table 1. Mesh dependency results in accuracy.

No	Number of elements	T_h (C°)	Percentage error (%)
a	23186	334.121	0.45%
b	703974	332.602	0.43%
c	116790	331.159	0.31%
d	183934	330.389	0.23%
e	215239	330.121	0.08%

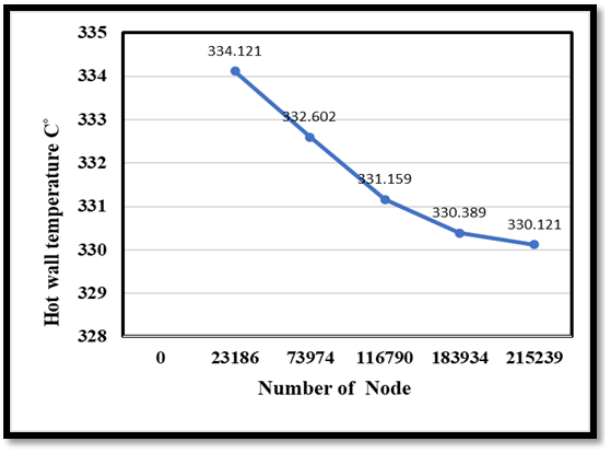

Figure 2. Variation of hot wall temperature with total number of elements.

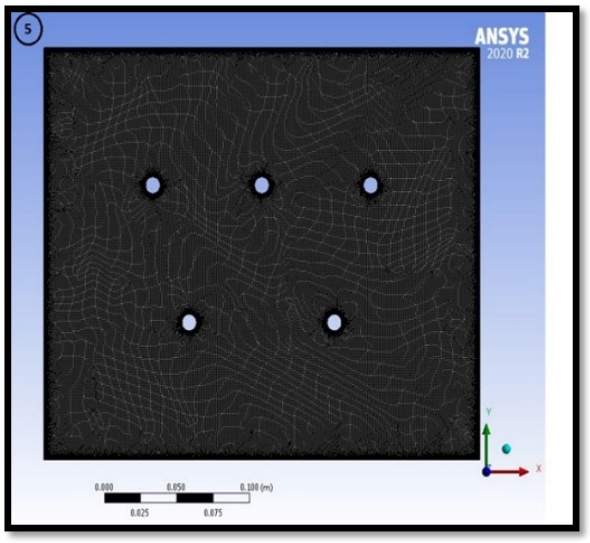

Figure 3. Variation of mesh density with number of elements.

Without appropriate boundary conditions, the governing differential equations for the situation at hand cannot be solved. Defining the proper boundary conditions is critical for numerical simulation work. The symmetry border is utilized in issues to reduce computing effort. The boundary conditions are chosen and illustrated in Table (2). The processes' boundary conditions are as follows

Table 2. Boundary conditions.

No.	B. Name	Material	Mom. B.C.	Thermal Boundary condition
1	Heater	Cupper	Wall	Heat flux
			No slip wall	q''=400, 600, 900 W/m^2
2	Top movable wall	aluminum	Wall	Static temperature
			U= 0.1, 0.2 m/s	300
3	Bottom, left and right walls	aluminum	Wall	Heat flux
			No slip wall	q''=0
4	Obstacle cylinders	Clear Acrylic Sheet	Wall	Heat flux
			No slip wall	q''=0

The finite volume method (FVM) was employed in this study to discretize the governing partial differential equations, yielding a set of linear algebraic equations. The field governing equations are solved using the commercial CFD solver ANSYS FLUENT (version 20). A discretization using the finite volume approach is based on an integral form of the partial differential equation to be solved (mass, momentum, or energy conservation rules). These equations are then discretized to generate a numerical analog. After that, the domain is separated into little grids or elements. The pressure values are obtained using the PRESTO (pressure staggering option) system, and the interaction between pressure and velocity is coupled using SIMPLIE (Semi - Implicit Method for Pressure Linked Equations). Lastly, the initial and boundary conditions of the particular problem are employed to solve these equations. The method of solution can be direct or iterative. Furthermore, some control parameters are employed to control the method's convergence, stability, and accuracy. For the momentum and energy variables, a second-order upwind technique was used, and SIMPLIE (Semi - Implicit Method for Pressure Linked Equations) was used to couple the interaction between pressure and velocity. The tolerance for continuity and velocity was set to ($1x10^6$) while the tolerance for energy was set to ($1x10^8$).

3. Results and Discussion

Under the operating conditions and physical properties mentioned in previous sections, 2D dynamic simulations for the enclosure with and without obstacles. The present work performs a numerical approach to study the temperature and velocity distribution in a square lid-driven enclosure. The enclosure with a length of 30 cm and width of 25 cm was built and has five interior adiabatic cylinders with a diameter of 1 cm. The enclosure's bottom wall is maintained at a high temperature of T_h, while the left and right walls are fully insulated. The enclosure's top wall is isothermally cooled at Tc and moves at a constant speed of U. The isotherm lines for two different heat source values (Q=400, 900W) (without motion for the top wall) were presented in Fig. (4). It was used to visualize the temperature line distribution inside the enclosure without obstacles. It is observed that the temperature contours stratified align the heater in the enclosure, and the thermal boundary layer was very thick due to the lack of cell circulation within the grove area. It is noticed that at V=0 m/s, the high values of temperature are at the bottom of the enclosure near the heated lower wall, due to there being no movement of the fluid inside the enclosure in all cases studied. It is noticed that when (V=0.1 m/s) for the top wall will affect the temperature and velocity lines distribution at (Q=400 W). However, due to the presence of speed, the flow becomes more distributed, and the boundary layer for temperature becomes thinner near the bottom wall of the enclosure. The temperature begins to decrease and the isotherm lines are concentrated on the lower left side of the enclosure. Note that the temperature values increase with an increase in the heat source values (Q=600,900W). As for velocity lines, due to the movement of the top wall note that the contours began to generate a large cell of circulation inside the enclosure region on the right upper

side near the top wall moveable and noticed that not affected by changing values heat sources (Q=600,900W).

In Fig (5) when the velocity equals (V=0.2 m/s), it is observed the temperature values began the decrease at any values of the heat source (400 and 900W) compared with the cases when (v=0, 0.1m/s), due to the movement of the upper wall, which works to reduce the temperatures inside the enclosure, and the thermal boundary layer was very thin, and the contours of velocity and stream function began to generate a large cell of circulation near of the top wall movable.

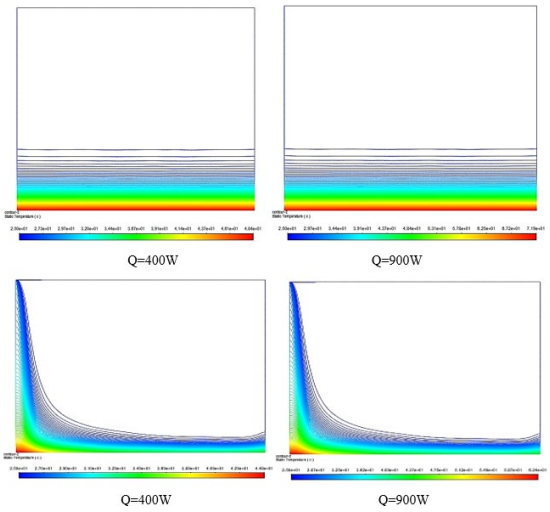

Figure 4. Isotherms lines for three heat sources different for without obstacle case at V=0 m/s (without motion for the top wall). V=0.1 m/s

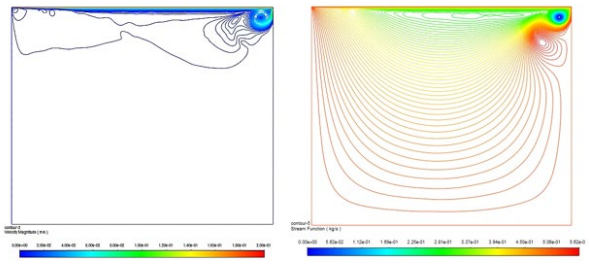

Figure 5. Isotherms, Velocity lines, and stream function for three heat sources different from without obstacle at V=0.2 m/s.

The isotherm lines for three different heat source values at (V=0 m/s) were presented in Fig. (6). It was used to visualize the temperature line distribution inside the enclosure with obstacles. It is noticed that at V=0 m/s, the high values of temperature are distributed, and the boundary thermal layers presented align the heated wall for the three different values heat source (Q=400,900 W). The circulating cell formed only in the cases of the presence of movement of the upper wall at (V=0.1,0.2 m/s) as shown in stream function and velocity vector. It is observed temperature values for those with obstacles are less in comparison with cases without obstacles. Fig (7) show that the enclosure isotherm contours distributed only on the left side of the enclosure at (V=0.1 m/s), High-value contours are limited to regions near the heated wall, whereas low-value contours dominate the rest of the enclosure, as a result of flow influence on the enclosure's circulation cell. Due to the presence of the obstacles, more distributed contours. The isotherm contours show a low value extending to the right end of the heated wall, while the high-valued contours mainly align to the left side of the heated wall. Fig (8) the results showed that the presence of obstacles will generate more than one cell of vortices inside the enclosure especially near the top wall movable due to the convection current, and the thermal boundary layer becomes very thin when the (V=0.2 m/s), it is observed the temperature values began in the decrease at any values of the heat source (Q=400,600,900W).

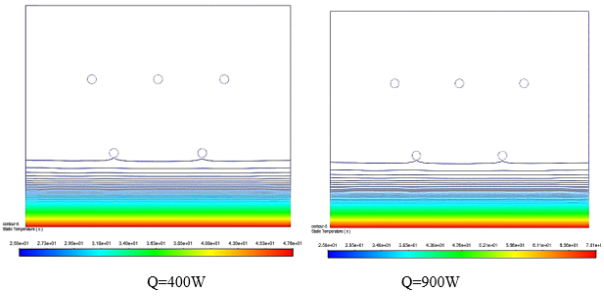

Figure 6. Isotherms lines for three heat sources different for with obstacle case at V=0 m/s (without motion for the top wall).

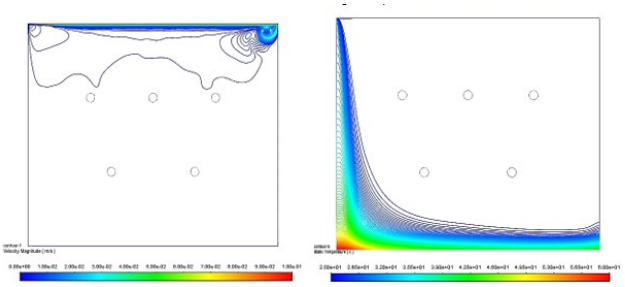

Figure 7. Isotherms, Velocity lines, stream function, and velocity vectors for three heat sources different from with obstacle at v=0.1 m/s.

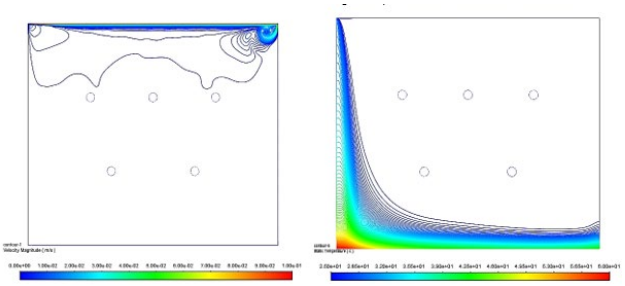

Figure 8. Isotherms, Velocity lines, stream function, and velocity vectors for three heat sources different from with obstacle at v=0.1 m/s.

Fig (9) shows the isotherm contours and stream function for the enclosure with obstacle radius (r=1,1.5, 2 cm), velocity top wall (V=0.2 m/s), and heat source values(Q=900W), from these results is observed that the temperature values decreasing when the radius of obstacle increase compared with the (r=0.5 cm), and the high valued contours mainly adhere to the regions near the hot wall(bottom) while low-value contours dominate the other regions of the enclosure. For stream function at (Q=900W), (V=0.2 m/s) and obstacle radius (r=1, 1.5, 2 cm) on formation a circulating cell big encompassing nearly the entire enclosure and extension to the obstacles due to increase in the heat transfer these results shows the effect the size radius to the heat transfer.

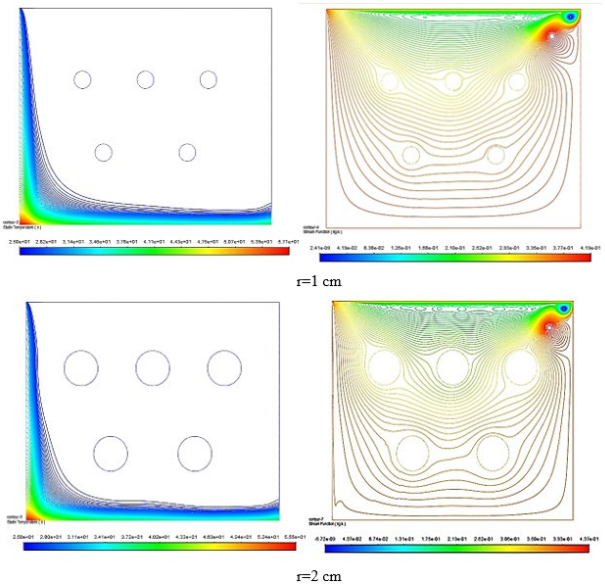

Figure 9. Isotherms and stream function for enclosure with obstacle at V=0.2 m/s and Q=900W.

Fig. (10) represents the Isotherm lines and stream function for the enclosure containing obstacles in different shapes at V=0.2 m/s and Q=900W. It is observed that the values of the temperature inside the enclosure for the obstacle that shapes a square are higher in comparison with the triangle and circler. From this concluded that the best shape of the obstacle must be a circle, so it was adopted experimentally due to it will increase from the heat transfer. Also, it showed that the distribution of the stream function from these results was noticed that be a vortex big near the top wall movable and the extent of the impact of the shape of obstacles inside the enclosure to the heat transfer.

Fig. (11) shows the Isotherm lines and stream function for an enclosure containing obstacles in different numbers and locations at V=0.2 m/s and Q=900W. However, it is noticed that the values of the temperature inside the enclosure decrease when the number of obstacle increase, and from this it is concluded that when the number of obstacles increases the heat transfer (the average Nussle number) increase inside the enclosure and the best heat transfer be when the n=4. It represents the distribution of the stream function from these results notice that be a vortex big near the top wall movable and the extent of the impact of the number and location of obstacles inside the enclosure.

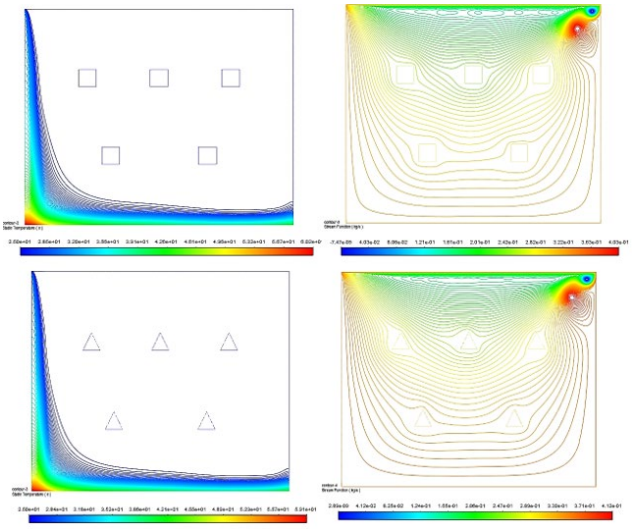

Figure 10. Isotherm lines and stream function for enclosure with obstacle square, triangle, and circle at V=0.2 m/s and Q=900W.

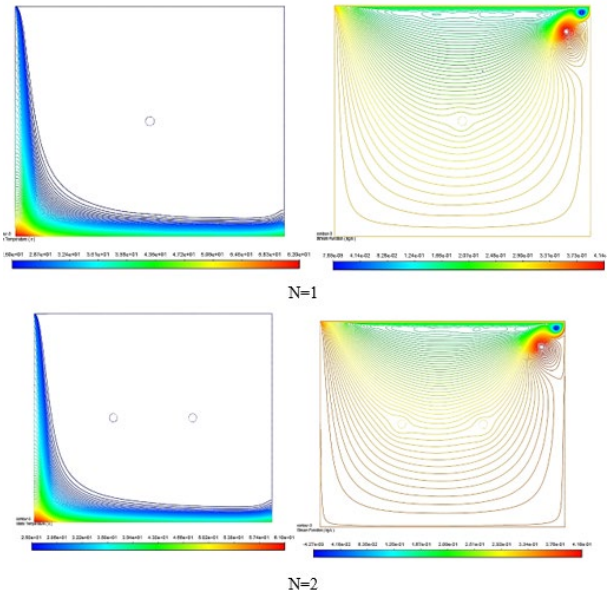

Figure 11. Isotherms and stream function for enclosure contains obstacles in different numbers and locations at V=0.2 m/s and Q=900W.

Fig. (12) shows the variation of the Nusselt number with the time inside the enclosure with obstacles at (r=0.5,1,1.5 and 2 cm) when the speed is equal to (V=0.2 m/s) for value to the heat source (Q=900W). The results of this outcome show that the presence of the obstacle results in an increase in the average Nusselt number compared with a case with no obstacle, increasing the values Nusselt number with an increase in the radius of the obstacle. The average increases are 10.4%,12%, 16%, and 19% compared with the case without the obstacle for radius values (r=0.5,1,1.5 and 2 cm). The results indicate that addition the of obstacles can be very useful in achieving a higher rate of heat transfer compared to without obstacles and the thermal behavior of birds changes as the diameter increases because less fluid area is occupied inside the enclosure.

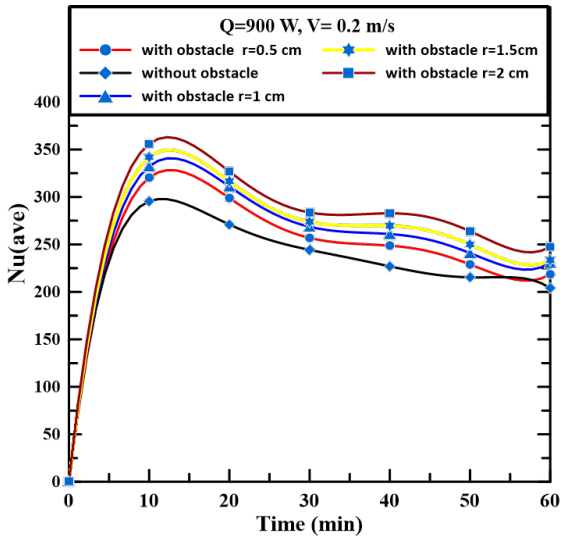

Figure 12. Nusselt number variation with time for the enclosure with and without obstacle at Q=900 W, V=0.2 m/s.

Fig. (13) shows the variation of the Nusselt number with the time inside the enclosure with obstacles with different shapes such as the circler, triangle, and square at the heat source Q=900W, V=0.2 m/s. As opposed to a situation without barriers, the results of this amount demonstrate that the existence of obstructions causes an increase in the average Nusselt number. When compared to triangular and square shapes, the obstacle with a circular shape has a larger average Nusselt number. Finaly the enhancement of Nusselt number is given by 16, 13, 11 % for obstacle models of circle r=1 cm, triangle and square respectively

Fig. (14) represents the variation of the average Nusselt number values inside an enclosure that contains obstacles in different numbers and locations at the heat source (Q=900W), V=0.2 m/s, and r=0.5 cm. From these results, it can be observed that the heat transfers (the average Nusselt number) increase when the number of obstacles increases inside the enclosure.

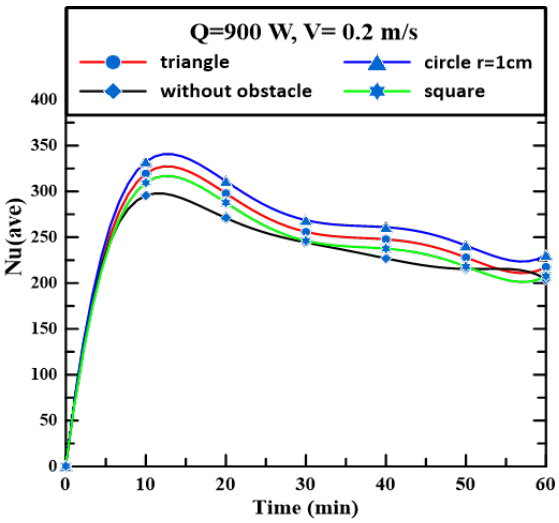

Figure 13. The average Nusselt number variation with time for the enclosure contains different shapes of the obstacle at Q=900 W, V=0.2 m/s.

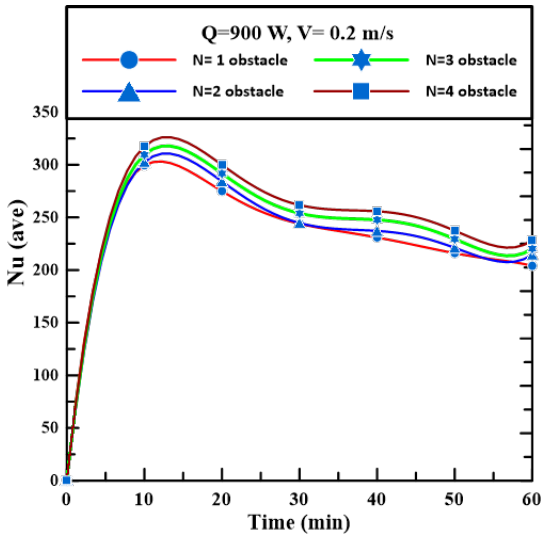

Figure 14. The average Nusselt number variation with time for the enclosure contains different numbers and locations of the obstacle at Q=900 W, V=0.2 m/s.

4. Conclusions

This study examines various computational fluid dynamics (CFD) models to analyze heat transfer and water flow via mixed convection in an enclosure with a moving wall under turbulent fluid flow conditions. The meshes were designed with the AutoCAD software, and the meshes, transport equations, and results were simulated using ANSYS©FLUENT. The dimensions of each of the five adiabatic cylindrical obstacles in the cage are 25 cm for width and 30 cm for length. Enclosures on the right and left are totally insulated; the top wall is retained at Th and functions as a working fluid while the

bottom wall is cooled isothermally at Tc and flows at a variable speed of U. The three types of obstacles used in this study were square, triangle, and circle (r=0.5,1,1.5, and 2 cm).

1. The use of five circular obstacles at r=2 cm improved the Nusselt number by 23%, and at r=0.5 cm, it rose by 8%.
2. For circles at r=1 cm, the Nusselt number improved by 13%, for triangles by 9%, and for square barriers by 3%.
3. The average increases in Nusselt number were 10.4%,12%, 16%, and 19%, compared with the case without the obstacle for radius values (r=0.5,1,1.5 and 2 cm) respectively.
4. The addition of obstacles can be very useful in achieving a higher rate of heat transfer compared with the case to without obstacles.
5. The existence of obstructions causes an increase in the average Nusselt number.
6. When compared to triangular and square shapes, the obstacle with a circular shape has a larger average Nusselt number.
7. Finally, the enhancement of Nusselt number is given by 16, 13, 11 % for obstacle models of circle r=1 cm, triangle and square respectively.

Conflict of interest

The authors have no conflict of interest to declare.

Acknowledgements

We are grateful for the laboratory support provided for this work by the Technical Engineering College-Baghdad, Middle Technical University, Iraq & Technical Engineering College-Mosul, Northern Technical University, Iraq.

Funding

The authors received no specific funding for this work.

References

Abedalh, A. S., Yasin, N. J., & Ameen, H. A. (2021). Thermal performance of HAVC system using heat pipe heat exchanger. *Journal of Mechanical Engineering Research and Developments*, *44*(2), 1-9.

Abdallah, A.S., Yasin, N.J., Ameen, H.A. (2022). Thermal performance enhancement of heat pipe heat exchanger in the air-conditioning system by using nanofluid. *Frontiers in Heat and Mass Transfer*, *18(1)*, 1-7.
https://doi.org/10.5098/hmt.18.10

Abedalh, A. S., Hussein, A. T., & Yousif, A. A. (2023). Experimental investigation for vapor compression system performance enhancement through condenser cooling by using shallow fluidized bed. *Journal of Thermal Analysis and Calorimetry*, *148*(21), 12301-12310.
https://doi.org/10.1007/s10973-023-12495-5

Abedalh, A. S., & Mohammed, S. H. (2023). Numerical Investigation Thermal Performance of Solar Air Heater Using Different Angle V-Grooved of Corrugated Absorber Plate. *Frontiers in Heat and Mass Transfer*, *21*, 227-243.
https://doi.org/10.32604/fhmt.2023.041777

Boidin, R., Halenkovič, T., Nazabal, V., Beneš, L., & Němec, P. (2016). Pulsed laser deposited alumina thin films. *Ceramics International*, *42*(1), 1177-1182.
https://doi.org/10.1016/j.ceramint.2015.09.048

Gangawane, K. M., Oztop, H. F., & Ali, M. E. (2019). Mixed convection in a lid-driven cavity containing triangular block with constant heat flux: Effect of location of block. *International Journal of Mechanical Sciences*, *152*, 492-511.
https://doi.org/10.1016/j.ijmecsci.2019.01.020

Hussein, A. T., Abedalh, A. S., & Alomar, O. R. (2023). Enhancement performance of vapor compression system using nano copper oxide lubricant inside compressor and a fluidized bed for condenser cooling. *Case Studies in Thermal Engineering*, *44*, 102819.
https://doi.org/10.1016/j.csite.2023.102819

Islam, A. W., Sharif, M. A., & Carlson, E. S. (2012). Mixed convection in a lid driven square cavity with an isothermally heated square blockage inside. *International journal of heat and mass transfer*, *55*(19-20), 5244-5255.
https://doi.org/10.1016/j.ijheatmasstransfer.2012.05.032

Kahveci, K., & Ogut, E. B. (2011). Mixed convection of water-based nanofluids in a lid-driven square enclosure with a heat source. *Heat Transfer Research*, *42*(8). https://doi.org/10.1615/HeatTransRes.2012003587

Khanafer, K., & Aithal, S. M. (2013). Laminar mixed convection flow and heat transfer characteristics in a lid driven cavity with a circular cylinder. *International Journal of Heat and Mass Transfer*, *66*, 200-209. https://doi.org/10.1016/j.ijheatmasstransfer.2013.07.023

Mamun, M. A. H., Rahman, M. M., Billah, M. M., & Saidur, R. (2010). A numerical study on the effect of a heated hollow cylinder on mixed convection in a ventilated cavity. *International Communications in Heat and Mass Transfer*, *37*(9), 1326-1334. https://doi.org/10.1016/j.icheatmasstransfer.2010.07.019

Messaoud, H., Bachir, M., & Djamel, S. (2017). Numerical study of mixed convection and flow pattern in various across-shape concave enclosures. *International Journal of Heat and Technology*, *35*(3), 567-575. https://doi.org/10.18280/ijht.350313

Morshed, K. N., Sharif, M. A., & Islam, A. W. (2015). Laminar mixed convection in a lid-driven square cavity with two isothermally heated square internal blockages. *Chemical Engineering Communications*, *202*(9), 1176-1190. https://doi.org/10.1080/00986445.2014.912634

Moukalled, F., Mangani, L., Darwish, M. (2016). The Finite Volume Method. In: The Finite Volume Method in Computational Fluid Dynamics. Fluid Mechanics and Its Applications, vol 113. Springer, Cham. https://doi.org/10.1007/978-3-319-16874-6_5

Moumni, H., Welhezi, H., Djebali, R., & Sediki, E. (2015). Accurate finite volume investigation of nanofluid mixed convection in two-sided lid driven cavity including discrete heat sources. *Applied Mathematical Modelling*, *39*(14), 4164-4179. https://doi.org/10.1016/j.apm.2014.12.035

Ouahouah, A., Kherroubi, S., Labsi, N., & Benkahla, Y. K. (2019). Mixed Convection in a Square Cavity with Anisothermally Heated Square Blockage and Filled with a Nanofluid. In *2nd National Conference on Computational Fluid Dynamics & Technology*. https://dx.doi.org/10.2139/ssrn.3372316

Shaalan, Z. A., Abedalh, A. S., & Hamadalla, M. W. (2021). Heat pump performance enhancement by using a nanofluids (experimental study). *Journal of Mechanical Engineering Research and Developments, 44 (2)*, 1-9.

Shirani, N., Toghraie, D., & Rostami, S. (2021). Comparative study of mixed convection heat transfer of water–Cu nanofluid in an enclosure having multiple rotating circular cylinders with different configurations and considering harmonic cylinders rotation. *Journal of Thermal Analysis and Calorimetry*, *144*, 1557-1570. https://doi.org/10.1007/s10973-020-09624-9

Yasin, N. J. Y. J., Alwan, D. A. D. H., & Abdulla, A. S. (2014). Experimental Study of Mixed Convection in an Enclosure with a Cold Movable Top Wall and Hot Bottom Wall. *Al-Khwarizmi Engineering Journal*, *10*(1), 32-46.

Yasin, N. J., Jehhef, K. A., & Abedalh, A. S. (2019). Experimental and theoretical study of heat pump performance enhancement by using a nanorefrigerantS. *Technology*, *10*(1), 25-42.

Yunus, A. C. (2003). Heat transfer: a practical approach, *MacGraw Hill N. Y.*, vol. 210.

Yousefzadeh, S., Rajabi, H., Ghajari, N., Sarafraz, M. M., Akbari, O. A., & Goodarzi, M. (2020). Numerical investigation of mixed convection heat transfer behavior of nanofluid in a cavity with different heat transfer areas. *Journal of Thermal Analysis and Calorimetry*, *140*, 2779-2803. https://doi.org/10.1007/s10973-019-09018-6